

# Surf-Deformer: Mitigating Dynamic Defects on Surface Code via Adaptive Deformation

Keyi Yin<sup>1</sup>, Xiang Fang<sup>1</sup>, Travis Humble<sup>2</sup>, Ang Li<sup>3</sup>, Yunong Shi<sup>4</sup>, and Yufei Ding<sup>1</sup>

<sup>1</sup>University of California, San Diego, CA, USA

<sup>2</sup>Oak Ridge National Laboratory, Oak Ridge, TN, USA

<sup>3</sup>Pacific Northwest National Laboratory, Richland, WA, USA

<sup>4</sup>AWS Quantum Technologies, New York, NY, USA

**Abstract**—In this paper, we introduce Surf-Deformer, a code deformation framework that seamlessly integrates adaptive defect mitigation functionality into the current surface code workflow. It crafts several basic deformation instructions based on fundamental gauge transformations, which can be combined to explore a larger design space than previous methods. This enables more optimized deformation processes tailored to specific defect situations, restoring the QEC capability of deformed codes more efficiently with minimal qubit resources. Additionally, we design an adaptive code layout that accommodates our defect mitigation strategy while ensuring efficient execution of logical operations.

Our evaluation shows that Surf-Deformer outperforms previous methods by significantly reducing the end-to-end failure rate of various quantum programs by 35× to 70×, while requiring only about 50% of the qubit resources compared to the previous method to achieve the same level of failure rate. Ablation studies show that Surf-Deformer surpasses previous defect removal methods in preserving QEC capability and facilitates surface code communication by achieving nearly optimal throughput.

## I. INTRODUCTION

Device errors significantly hinder the advancement of quantum computing [3], obstructing its capability to fulfill its vast potential [4], [5], [6]. Consequently, Quantum Error Correction (QEC), a technique that protects quantum information by using redundant qubits, is pivotal to achieve scalable fault-tolerant quantum computing (FTQC) [7].

Among current QEC code proposals [8], [9], [10], [11], [12], [13], [14], *surface code* [10], [14], [15], [16] is a leading candidate to achieve FTQC due to its simple 2D-lattice topology and high tolerance to physical qubit errors. Due to their practicality, small-scale surface codes have been successfully demonstrated on several quantum computing platforms [17], [18], [19], [20].

However, scaling surface codes still presents several challenges, especially *dynamic defects* that emerge on quantum hardware during computation. Events like cosmic-ray strikes on superconducting devices can induce multi-bit burst errors (MBBEs) during computation, leading to defects with localized error rate spikes as high as 50% in affected regions [21], [22], [23], [24]. *Leakage errors* in all platforms remove the qubit states from the computation space, rendering them inoperable and triggering high-weight correlated errors [25], [26]. Various factors [27], [28], [29] can cause *error drift* that increases the qubit error rate on different quantum platforms.

These defects can persist for thousands of QEC rounds before their effects go away [22], severely compromising the error correction capability of surface codes. Without mitigation, the logical error rate could potentially increase by a factor of 100 on average [2], [17]. Hence, it is imperative to develop appropriate mitigation strategies for dynamic defects to maintain surface codes' error correction ability.

Dynamic defects are an inherent aspect of quantum device physics, rendering them insurmountable through hardware mitigation alone [24], [30]. Thus, mitigation at the software level is crucial. Current hardware detectors [31], [32] can swiftly and accurately detect these defects using statistical methods. Using these defect data, software-level solutions can be developed to effectively manage dynamic defects. Currently, the two main software approaches for defect mitigation are *defect removal* and *code enlargement*, although each method comes with its own challenges.

**A. Defect Removal** excludes defective qubits from syndrome measurements during QEC cycles to ensure the accuracy of decoding and subsequent correction. One leading defect removal technique is the state-of-the-art *Adaptive Surface Code* [1](ASC-S) with the boundary transformation of rotated surface code [33], which performs a simple transformation (known as *super-stabilizer* [34], [35], [36], [37], [38]) for defect removal. Defect removal methods such as ASC-S face two issues:

(1) *Lack of Distance Recovery*: Defect removal methods remove defective qubits without introducing new ones, leading to a permanent reduction in code distance (section II-A) and increasing program failure rate. Preemptively selecting a larger code size could mitigate this issue to some extent, but accurately allocating the right qubit resources for all defect patterns is a challenge, often resulting in either insufficient resource allocation or wastage of qubits.

(2) *Inability to Address Different Defect Types*: Defects in surface codes appear as either defective syndrome or data qubits and they can be further categorized by their spatial location as boundary, corner, and interior qubits. Current methods apply a uniform transformation to all defects, hindering them from addressing specific defect types, which leads to suboptimal error correction capability in the resulting code.

**B. Code enlargement** preserves the code distance under defects by scaling up the code size. As an example, Q3DE [2], a

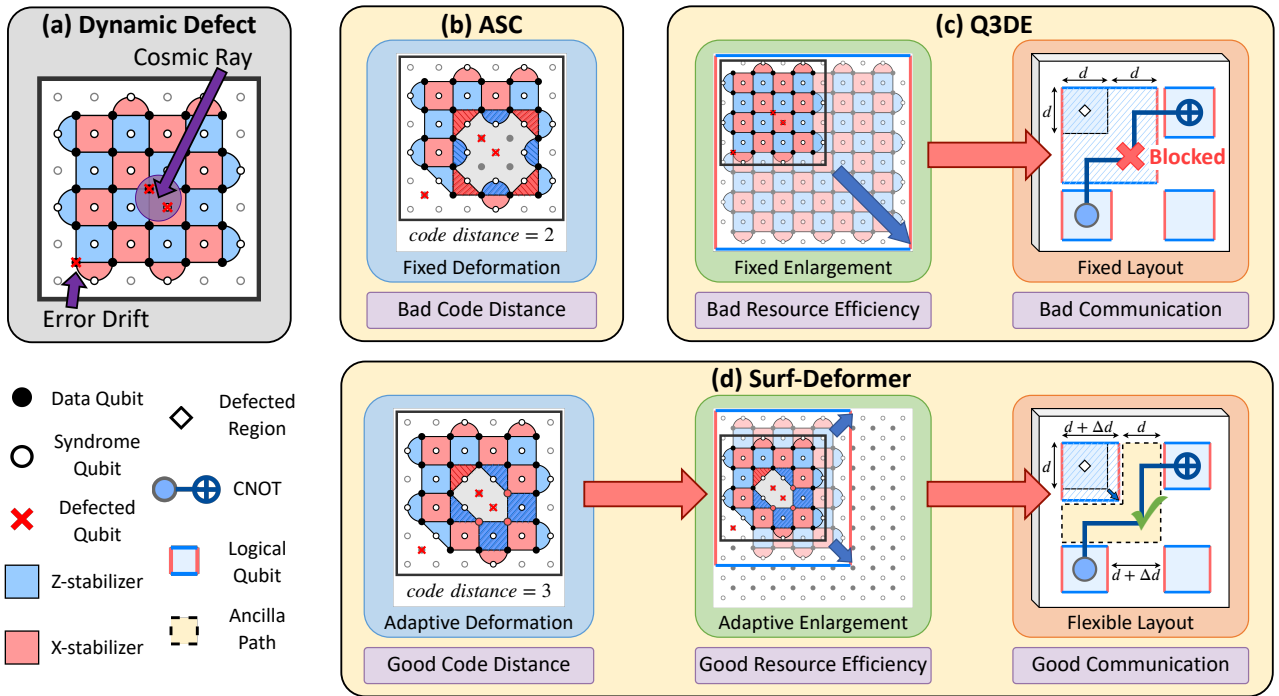


Fig. 1. Comparison of Surf-Deformer with existing dynamic defect mitigation methods. (a) Illustration of dynamic defects induced by cosmic rays or error drift. (b) Adaptive Surface Code (ASC-S) [1] employs fixed deformation operation that leads to bad code distance. (c) Q3DE [2] utilizes fixed-scale enlargement on a fixed layout, resulting in poor resource utilization and communication efficiency. (d) Surf-Deformer enables adaptive defect removal, enlargement, and layout optimization, providing a more versatile and efficient response to dynamic defects.

leading enlargement method, initially spaces surface code patches by the code distance  $d$  (fig. 1(c)). It then enlarges the code to a fixed size of  $2d$  after defect detection (fig. 1(c)), borrowing the “growth” transformation designed for *lattice-surgery* based logical operations [39]. Despite its simplicity, the Q3DE approach suffers from several drawbacks:

- (1) *Increased Logical Error Rate*: Q3DE’s fixed-size enlargement cannot accommodate defect removal, allowing defects to persist and their errors to spread through surface code syndrome measurements, which leads to a significant increase in logical error rates (as detailed in section II-A).
- (2) *Qubit Resource Inefficiency*: Due to the lack of guarantee of the logical error rate, Q3DE pessimistically doubles code size after defects are detected, irrespective of their specific patterns. This often results in excessive enlargement beyond what’s needed for code distance restoration, leading to poor qubit resource efficiency.
- (3) *Communication Impediment*: Q3DE focuses on recovering single code patches but overlooks the fact that doubled-size codes occupy the space between surface codes. This space is crucial for logical qubit communication in logical operations. This limitation results in significantly limited end-to-end system efficiency.

At a high level, the challenges faced by current defect removal and enlargement approaches arise from their simple application of existing deformation methods, such as super-stabilizer and fixed-size enlarging. This rigid application limits their capacity to handle various defect types, enlarge incre-

mentally, and integrate with each other effectively, resulting in high logical error rates.

Prompted by these challenges, we introduce Surf-Deformer, a code deformation framework that extends the current surface code instruction set [40], [41], [42], [43] (detailed in section II-D) to include adaptive defect mitigation capabilities. Surf-Deformer meticulously crafts four deformation instructions (section IV) that provides superior granularity and versatility compared to fixed operations in ASC-S and Q3DE.

Surf-Deformer consists of two components: a compile-time *layout generator* and a runtime *code deformation unit*. The code deformation unit uses the extended instruction set to implement a highly optimized deformation strategy that unifies the defect removal and the enlargement approaches. This unified approach eliminates error sources from defects while restoring code distance, overcoming the limitations of ASC-S and Q3DE (Issue A.(1), B.(1)). Furthermore, due to Surf-Deformer’s instruction design, the code deformation unit can effectively manage various defect types and facilitate adaptive enlargement, substantially improving error correction capabilities and resource efficiency (Issue A.(2), B.(2)). Additionally, the layout generator strategically adjusts the spacings between logical qubit patches to ensure unimpeded execution of two-qubit logical operations, thereby maintaining high end-to-end system efficiency (Issue B.(3)). As a result, Surf-Deformer resolves all issues of previous methods.

We perform a comprehensive evaluation of Surf-Deformer. The end-to-end performance on various quantum programs

shows that Surf-Deformer considerably suppresses the program’s failure rate by  $35\times \sim 70\times$  compared with ASC-S in [1], [33] while maintaining nearly-optimal runtime, and requires only  $\sim 50\%$  of Q3DE’s qubit resources. Ablation studies show that our framework significantly outperforms previous defect removal methods in preserving code distance and facilitates surface code communication by achieving nearly optimal throughput.

Our contributions can be summarized as follows:

- We introduce Surf-Deformer, a deformation framework designed for adaptive defect mitigation on surface codes. [link]
- We propose four meticulously crafted deformation instructions, offering highly flexible deformation strategies.
- We establish a novel code deformation strategy based on our instructions, which not only unifies previous defect removal and enlargement methods but also yields more optimized deformation processes.
- We propose a novel surface code layout that achieves nearly optimal runtime while maintaining the target logical error rate, effectively resolving communication issues present in existing methods.

## II. BACKGROUND AND MOTIVATION

### A. Surface Codes

Surface codes arrange physical qubits on a 2D grid to collectively encode logical qubits. We illustrate its key components below as well as in fig. 2.

*Pauli operators.* Pauli  $X$  and  $Z$  operators are fundamental qubit operations in QEC for describing both errors and error detection operations [44]. Importantly,  $X$  and  $Z$  anti-commute, i.e.,  $XZ = -ZX$ , allowing QEC codes to detect  $X$ - or  $Z$ -errors using the Pauli  $Z$  or  $X$  operator. Additionally,  $X$  or  $Z$  errors can be corrected by applying the  $X$  or  $Z$  operator because  $X^2 = Z^2 = I$ .

*Data and Syndrome qubits.* Physical qubits in surface codes are either data qubits or syndrome qubits. Data qubits (black dots) store the logical quantum state, while syndrome qubits (white dots) are for error detection of adjacent data qubits through stabilizer measurements.

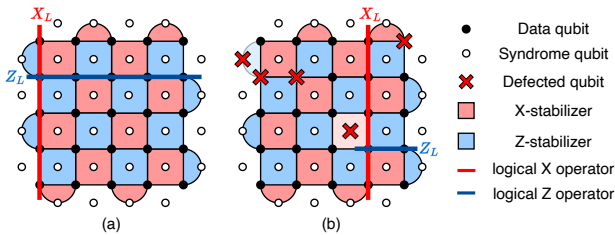


Fig. 2. (a) A surface code logical qubit with code distance 5. (b) A defective surface code logical qubit with code distance reduced to 2, illustrated by the weight-2  $Z$  logical operator.

*Stabilizers.* Each syndrome qubit is associated with a *stabilizer* [45], [46], composed of Pauli operators on adjacent data qubits which identifies the type of error and the specific data qubits for which the syndrome qubit is accountable.

Interior and boundary surface code stabilizers measure four and two adjacent data qubits, respectively, depicted as squares for interiors and half-circles for boundaries. Stabilizers are distinguished into  $X$ -type (red boxes), which detect  $Z$  errors and  $Z$ -type (blue boxes), which detect  $X$  errors. Stabilizers are designed to commute, ensuring consistent error detection.

*Code distance* is the minimal number of physical errors that induce a logical operation (error). The code distance of a surface code equals to the number of data qubits on its edge (fig. 2(a)). A surface code with more physical qubits gives a larger code distance and has better error resilience [15], [47].

### B. Quantum Errors

*Physical Errors.* In QEC literature, physical errors typically refer to errors with a low error rate around  $10^{-3} \sim 10^{-4}$  and are detected indirectly through stabilizer measurements. Extensive research demonstrates that these physical errors can be effectively corrected by surface codes, resulting in an exponentially suppressed logical error rate as qubit redundancy increases. This applies to various error types, including stochastic errors (single-bit error, CNOT error, etc.) [15] and correlated, non-Markovian errors [48], [49]. Consequently, low-error-rate physical qubits continue to function correctly in the surface code due to QEC protection.

*Defects.* In contrast, defects are errors with a high error rate or those rendering qubits inoperable. Defects are classified as *static defects* (e.g., fabrication errors [37], [50], qubit loss [36], [51]) that happen before runtime, and *dynamic defects* (e.g., cosmic-ray events [21], [22], leakage [25], error drift [27]) that occur during runtime. These defects significantly compromise the functionality of surface codes. For instance, in fig. 2(b), defective syndrome qubits with high error rates fail to provide accurate error information, rendering the stabilizer inoperable and potentially reducing the code distance by half or more. Defective data qubits consistently generate excessive errors that can surpass the code’s QEC capability, elevating the logical error rate by orders of magnitude [2]. Therefore, excluding defects is crucial to maintaining the efficacy of surface codes. Fortunately, these defects can be detected directly using hardware technologies [31], [32] or indirectly through statistical methods [1], [2], enabling alternative strategies beyond standard QEC for addressing them.

### C. Gauge Transformation

This section introduces *gauge transformation* [52], [53], a fundamental technique that underpins Surf-Deformer. Since our goal is to perform runtime code deformation, it is crucial to preserve the information stored in the logical qubit. To achieve this, we formalize atomic gauge transformation instructions that adjust the stabilizers to be measured while maintaining the logical state encoded in the surface code.

*Gauge operators.* In classical QEC theory, introducing each stabilizer removes a degree of freedom from the system, allowing the remaining degrees of freedom to encode logical qubits. More generally, introducing fewer stabilizers can save degrees of freedom to encode *gauge qubits* in addition to logical

qubits. These extra degrees of freedom provide more flexibility in code design and can lead to better performance [54], [55]. Operations that change the states of *gauge qubits* without affecting logical qubits are called *gauge operators*. Notably, gauge operators form anti-commuting pairs but commute with the other stabilizers [53], [56]. Unlike stabilizers, they are not measured in every QEC cycle but can be measured in different cycles to collectively infer error information.

**Gauge Transformation** modifies the set of stabilizer and gauge operators to achieve greater flexibility for the surface code. This process can be broken down to four basic types, serving as atomic instructions for code deformation operations:

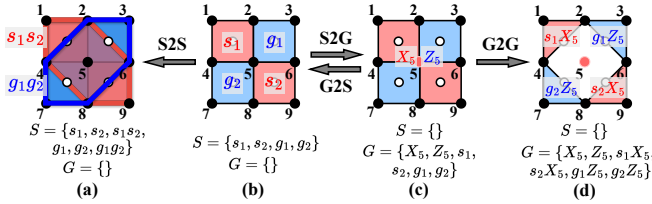


Fig. 3. Examples of basic gauge transformations.

(1) **Stabilizer to Gauge (S2G)**: S2G converts a stabilizer to a gauge operator. Specifically, we match the stabilizer with an new anti-commuting operator and they both become gauge operators. For example, in fig. 3(b),  $X_5$  anti-commutes with  $g_1, g_2$ , so stabilizers  $g_1, g_2$  are converted to gauge operators along with  $X_5$ . Likewise, Stabilizer  $s_1, s_2$  becomes gauge operators by adding new  $Z_5$ . As shown in in fig. 3(c), updated stabilizer and gauge set become  $S = \{\}$  and  $G = \{X_5, Z_5, s_1, s_2, g_1, g_2\}$ . This instruction creates degree of freedoms by introducing more gauge operators. Notably, S2G instructions are commutative, as they only depend on the set of newly introduced gauges.

(2) **Gauge to Stabilizer (G2S)**: G2S converts a gauge operator into a stabilizer by measuring it in every cycle and do correction based on the measurement result [57]. Accordingly, all gauge operators that anti-commute with it are removed from the gauge set because it should commute with all gauge operators to be a new stabilizer. G2S is the inverse process of S2G (fig. 3(b)(c)). This instruction eliminates degrees of freedom by introducing more stabilizers.

(3) **Stabilizer to Stabilizer (S2S)**: S2S multiplies two stabilizers to form a new stabilizer. For instance, in fig. 3(a), the product of stabilizers  $s_1, s_2$  and  $g_1, g_2$ , yields the stabilizers  $s_1s_2$  and  $g_1g_2$ . This instruction is often used to build larger stabilizers.

(4) **Gauge to Gauge (G2G)**: G2G multiplies two gauge operators to form a new gauge operator. For instance, in fig. 3, the products of gauge operators  $s_1X_5, s_2X_5, g_1Z_5$ , and  $g_2Z_5$  also result in gauge operators. This instruction reorganizes gauge operators, potentially separating some qubit from the code. For example, the G2G transformation in fig. 3(d) indicates that qubit  $q_5$  can be separated from the code, as the only remaining gauges operators acting on it are  $X_5$  and  $Z_5$ .

In summary, these four atomic instructions offer the building blocks for composing versatile and complex instructions to deform the surface codes for defect mitigation. For the proof

of how the gauge transformation preserves the logical state, we recommend referring to the appendix section in the arXiv version [58].

#### D. Quantum Program Execution on Surface Codes

To execute a high-level quantum program on surface codes [40], [41], [42], [43], a compile time *algorithm compiler* first maps algorithmic qubits to surface code patches and lowers the logical operations to a native instruction schedule. During runtime, an *execution unit* utilizes this instruction schedule along with real-time data (such as syndrome measurement results) to execute the program.

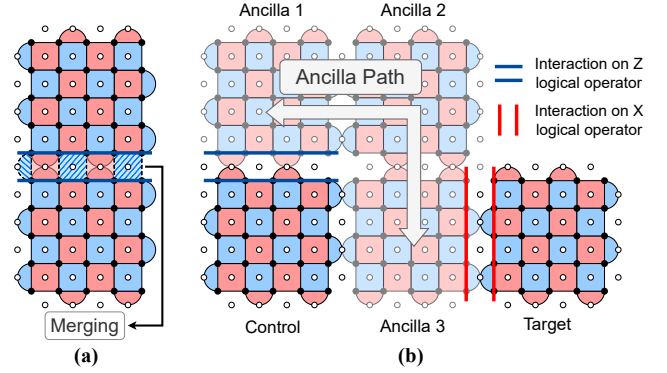


Fig. 4. (a) Example of merging two code patches. (b) Perform a logical CNOT gate on two distant logical qubits through an ancilla path. The control (resp. target) logical qubit interacts with the ancilla logical qubit on the edge of Z- (resp. X-) logical operators, with equal-length interacting edges.

**Instruction set.** Current implementations of surface code logical operations are mainly based on the Lattice Surgery (LS) method [39], which provides an instruction set to expand and connect surface code patches to update and entangle logical states [52]. These instructions, such as *grow*, *merge*, and *split*, are composed of the atomic instructions introduced in section II-C. For example, the *merge* instruction connects two arrays of physical qubit registers through a series of S2G and G2S transformations. In fig. 4(b), applying *merge* to the blue and red lines activates syndrome measurements on the ancillary patches between the logical surface code patches, facilitating a logical 2-qubit CNOT operation.

**Code layout.** Current surface code compilers as well as Q3DE arrange logical qubits on a grid with an inter-space of  $d$ , as shown in fig. 4(b). This layout ensures that activated ancillary patches for logical operations maintain the same code distance as logical qubits, providing same level of noise protection. Please refer to the introductory paper [59] for more details.

### III. THE SURF-DEFORMER FRAMEWORK

The Surf-Deformer framework consists of two main components: a compilation time *layout generator* and a runtime *code deformation unit*. As illustrated in fig. 5, Surf-Deformer integrates seamlessly with the existing surface code components, including the algorithm compiler and the execution unit.

**The layout generator** analyzes the input program to estimate the required number of logical qubits and the necessary



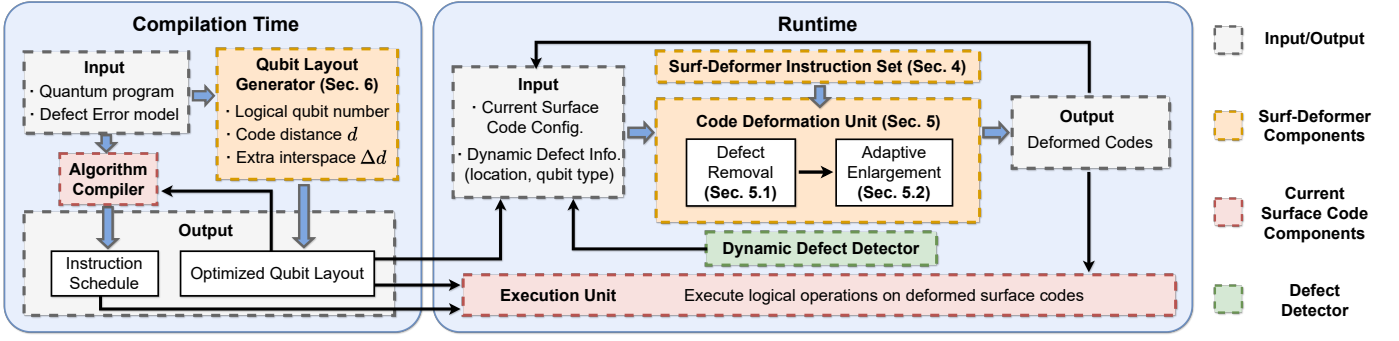


Fig. 5. Surf-Deformer integrates a Qubit Layout Generator during compilation time and a Code Deformation Unit during runtime into the current surface code workflow. They are combined to extend adaptive defect mitigation functionality to the existing surface code implementation.

code distance  $d$  to achieve a target logical error rate. It also computes the additional inter-space  $\Delta d$  based on the defect error model. This extra space accommodates potential enlargements and ensures communication between logical qubits during the execution of operations. We discuss the adaptive layout generator in detail in section VI.

**The code deformation unit** is the core component of Surf-Deformer. It deforms logical qubits dynamically to optimize defect mitigation during runtime. Utilizing real-time defect information from defect detectors and the current surface code configuration, the code deformation unit applies our adaptive deformation strategy. This strategy employs instructions from our extended instruction set to effectively remove defects and execute adaptive enlargements. The unit then forwards these instruction schedules to the execution unit for actual updates. Notably, despite the adaptiveness of our deformation methodology, actual code deformation updates can be implemented within a single QEC cycle.

We detail the extended instruction set in section IV and the code deformation unit in section V.

#### IV. THE SURF-DEFORMER INSTRUCTION SET

Previous methods ASC-S and Q3DE are limited by their simplistic and fixed deformation operations for diverse defect patterns. In response, Surf-Deformer introduces four carefully crafted instructions (table I) to extend the current surface code instruction set (section II-D). `DataQ_RM` and `SyndromeQ_RM` target the removal of interior data and syndrome qubits, respectively, while `PatchQ_RM` and `PatchQ_ADD` modify the boundaries of code patches to achieve adaptive boundary defect removal and code enlargement. Akin to CISC in classical computing, each instruction is constructed from multiple atomic instructions (section II-C) adapted for the surface code topology, as detailed in fig. 6. Meanwhile, these instructions are granular enough to ensure seamless integration and versatile enough to support a broad spectrum of deformation operations.

##### A. Code Deformation Instructions of Surf-Deformer

fig. 6 presents four deformation instructions introduced by Surf-Deformer. Physical qubits are denoted by lattice

TABLE I  
INSTRUCTION SETS OF VARIOUS SURFACE CODE IMPLEMENTATIONS

Method	Extended Instructions over LS	Supported Operations
Lattice Surgery	N/A	Logical operations
Q3DE	N/A	Logical operations, Fixed enlargement
ASC-S	<code>DataQ_RM</code>	Logical operations, Fixed qubit removal
Surf-Deformer	<code>DataQ_RM</code> , <code>SyndromeQ_RM</code> , <code>PatchQ_RM</code> , <code>PatchQ_ADD</code>	Logical operations, Adaptive qubit removal, Adaptive enlargement

coordinates, and boundaries by a list of qubit coordinates, both serving as input parameters of instructions.

**(a) Data qubit removal (`DataQ_RM`):** `DataQ_RM` removes a single data qubit. As shown in fig. 6(a), it first uses four `S2G` to convert stabilizers  $s_1, s_2, g_1, g_2$  into gauge operators, while introducing gauge operators  $Z_0, X_0$  that anti-commute with  $s_1, s_2$  and  $g_1, g_2$ , respectively. It then uses four `G2G` to adjust gauge operators  $s_1, s_2, g_1, g_2$  (rectangles) into  $X_0 s_1, X_0 s_2, Z_0 g_1, Z_0 g_2$  (triangles), effectively separating  $q_0$  from the code and enabling its removal. Notably, `DataQ_RM` coincides with ASC-S's super-stabilizer method for single data qubit removal. However, within our framework, `DataQ_RM` is constructed explicitly and could be combined with other instructions to perform more versatile deformations, as will be shown in section V.

**(2) Syndrome qubit removal (`SyndromeQ_RM`):** `SyndromeQ_RM` presents a novel method to remove a single syndrome qubit. It uses four `S2G` to form  $g_1 - g_4$ . Interestingly, these four gauge operators form a new stabilizer (blue octagon in fig. 6(b)) that doesn't rely on  $q_0$ . Meanwhile, four gauge operators  $X_1 - X_4$  are introduced (red dots), and their product forms a stabilizer  $X_{1,2,3,4}$ . Measurement of  $X_{1,2,3,4}$  can be achieved by using its constituent gauge operators without relying on the syndrome qubit  $q_0$ , which allows the removal of  $q_0$  from the code. This novel method maximizes the utility of adjacent intact data qubits and achieves optimal

removal of a single interior syndrome qubit. Additionally,  $\text{SyndromeQ\_RM}$  and  $\text{DataQ\_RM}$  commute, as they both exclusively utilize  $\text{S2G}$ , which commute with themselves. This commutativity enables  $\text{SyndromeQ\_RM}$  to be optimal even for complex defect patterns, as will be discussed in section V.

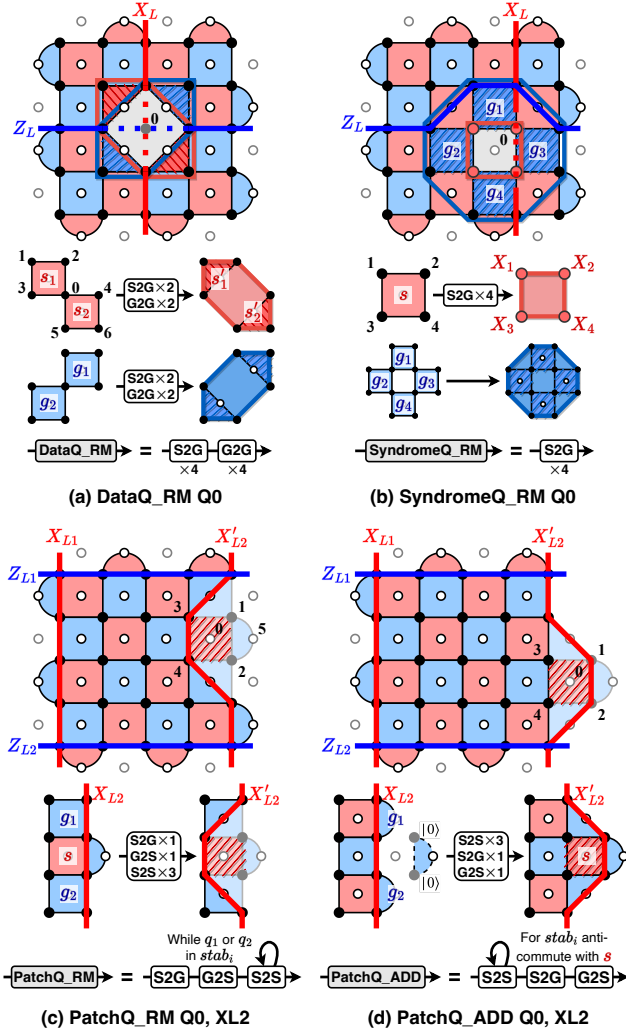


Fig. 6. Examples of the four deformation instructions of Surf-Deformer.  $Q_i$  is the coordinate of qubit  $q_i$  and  $XL_j$  is the coordinate that represents the boundary  $X_{Lj}$ .

**(3) Boundary qubit removal (PatchQ\_RM):**  $\text{PatchQ\_RM}$  removes defects on the boundary—e.g. the syndrome qubit  $q_5$  or data qubits  $q_1, q_2$  in fig. 6(c). This is achieved by combining several atomic instructions in section II-C to deform the boundary, thus excluding the defects from the code patch. fig. 6(c) presents an example where the boundary defective data qubit  $q_1$  is removed by deforming the boundary from  $X_{L2}$  to  $X'_{L2}$  (specifically, we add and fix  $Z_1$  as a stabilizer and update the rest of stabilizers and gauge operators accordingly).

**(4) New qubits incorporation (PatchQ\_ADD):** The instruction  $\text{PatchQ\_ADD}$  introduces new qubits beyond the original code. A new data qubit  $q$  is initialized in either the  $|0\rangle$  or  $|+\rangle$  state, equivalent to introducing a new stabilizer  $Z_q$  or  $X_q$ . New syndrome qubits are then added along with their

associated stabilizers, which update the stabilizers and gauge operators through a series of atomic instructions (section II-C), resulting in a deformed code containing additional qubits. fig. 6(d) presents an example of adding two data qubits and one syndrome qubit. This instruction can be iterated to facilitate code enlargement.

These four instructions can be combined to manage various defect types and facilitate adaptive code enlargement. The granularity and versatility provided by these instructions form the basis of our highly adaptive code deformation strategy, which will be detailed in section V.

---

#### Algorithm 1: Defect Removal Subroutine

---

**Input:** stabilizer set  $S$ , gauge set  $G$ , defective qubit set  $D$   
**Output:** stabilizer set  $S'$ , gauge set  $G'$

```

1 for  $d_i \in D$  do
2   if  $d_i \in \text{Interior\_Q}$  then
3     if  $d_i \in \text{Data\_Q}$  then
4       |  $\text{DataQ\_RM } d_i$ 
5     else
6       |  $\text{SyndromeQ\_RM } d_i$ 
7     end
8   else
9     if  $d_i \in \text{EdgeX\_Q}$  and  $d_i \in \text{EdgeZ\_Q}$  then
10      |  $p_X, e_X = \text{find\_patch}(d_i, X)$ 
11      |  $p_Z, e_Z = \text{find\_patch}(d_i, Z)$ 
12      |  $p, e = \text{balancing}(p_X, e_X, p_Z, e_Z)$ 
13    else if  $d_i \in \text{EdgeX\_Q}$  then
14      |  $p, e = \text{find\_patch}(d_i, X)$ 
15    else
16      |  $p, e = \text{find\_patch}(d_i, Z)$ 
17    end
18    |  $\text{PatchQ\_RM } p, e$ 
19  end
20 end
21 return  $\text{Distance}(S, G) - \text{Distance}(S', G')$ 

```

---

## V. THE CODE DEFORMATION UNIT

The code deformation unit is the core component of Surf-Deformer for adaptive defect mitigation. Before every QEC cycle, the code deformation unit receives the current surface code configuration (including the shape and location of logical qubit patches) from the last round of deformation and current defect information from the dynamic defect detector. Leveraging this information, the code deformation unit executes two subroutines sequentially, as illustrated in fig. 5. The first subroutine, *Defect Removal*, removes detected qubits from the current code. The second subroutine *Adaptive Enlargement* takes the resulting code, calculates the new code distance, and adaptively enlarges the code.

### A. Defect Removal Subroutine

The defect removal subroutine, outlined in algorithm 1, is crafted to strategically handle various types of defects. Below, we detail the components of this algorithm:

**Interior defect removal.** The first `if` branch handles interior defect removal. As shown in section IV, the optimal removal of defective interior qubits can be achieved simply by applying either `DataQ_RM` or `PatchQ_RM`, depending on the qubit type. This simple strategy also achieves optimal removal even for complex defect patterns, since `DataQ_RM` and `PatchQ_RM` commute. This commutativity ensures that the removal of neighboring qubits does not interfere with each other, preserving the optimality of the strategy.

**Comparison with ASC-S.** ASC-S solely employs the `DataQ_RM` instruction even for defective syndrome qubits. For removing a defective syndrome qubit, ASC-S must apply `DataQ_RM` four times to remove adjacent data qubits, even if they are not defective. This can result in an unnecessary loss of code distance. For example, the deformed code produced by ASC-S in fig. 7(a) has a Z-distance of only 3, while our strategy can preserve it to be 5.

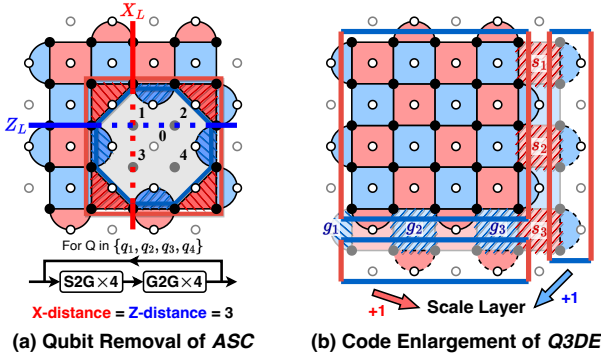


Fig. 7. Illustration of ASC-S and Q3DE. (a) The resulting code of ASC-S has X- and Z-distance both equal to 3, while our instruction fig. 6(b) leads to a code with Z-distance 5 and X-distance 3. (b) Code enlargement of Q3DE equates to multiple `PatchQ_ADD` instructions.

**Boundary defect removal.** The removal of boundary defective qubits is achieved through `PatchQ_RM` (fig. 6(c)). However, unlike the interior case where a larger stabilizer can be formed to provide additional error detection capabilities (fig. 6(a)(b)), simply applying `PatchQ_RM` leads to suboptimal code distance. Thus, we have to strategically apply `G2S` to introduce new stabilizers for extra protection. Especially in the corner case, we have to carefully choose from which edge to choose the gauge operator for conversion, to balance the distances X and Z. For example, for the defective data qubit  $q_0$  in the top right corner of fig. 8, we can convert either  $Z_q$  or  $X_q$  to a stabilizer. In the *balancing* function, we select the one that balances the X- and Z-code distances, reflected by the length of the boundaries (red and blue lines) to ensure that the deformed code remains resilient to both X- and Z-errors.

**Comparison with ASC-S.** ASC-S disables defective qubits on the boundary, disregarding their impact on the X-, Z-distances.

As fig. 8 shows, ASC-S converts the gauge operator  $Z_0$  into stabilizer to minimize the number of disabled qubits, leading to a smaller Z-code distance than Surf-Deformer.

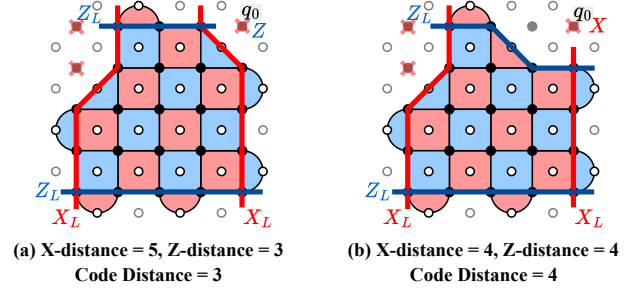


Fig. 8. Convert the right gauge operator into stabilizer to balance the X-, Z-distance. (a) ASC-S converts the gauge operator  $Z_0$  into stabilizer, leading to unbalanced X-, Z-distance and a smaller code distance. (b) Surf-Deformer converts the gauge operator  $X_0$  into stabilizer, leading to balanced X-, Z-distance and a larger code distance.

### B. Adaptive Enlargement Subroutine

This subroutine, outlined in algorithm 2, receives the deformed code of the *Defect Removal Subroutine* and efficiently restores the lost code distance by introducing new qubits.

**Code enlargement with defective patches.** After defect removal, we evaluate the reduction in both X- and Z-code distances compared to the ideal surface code. Calculating the code distance for every patch added to the surface code could be inefficient. In the `find_layer` function, we identify a set of patches, denoted as a *scale layer*, that can increase the code distance by at least one unit of the relevant type.

However, both boundary and new scale layers may contain defects, which requires adaptive enlargement. For example, in fig. 9(a), defective qubits  $q_1$  and  $q_2$  are removed, resulting in an irregular boundary that hinders regular enlargement. Similarly, in fig. 9(c)(d), the defective qubit  $q_0$  in the prospective scale layer also complicates the enlargement, since it need two scale layers to restore its  $Z_L$  distance of 5.

To solve this problem, Surf-Deformer combines the instruction `PatchQ_ADD` with the qubit removal subroutine `DataQ_RM`, `SyndromeQ_RM`, `PatchQ_RM`, as shown in line 24 in algorithm 2. Initially, defective qubits are temporarily disregarded to facilitate the regular enlargement. Subsequently, these defective qubits are excluded using our qubit removal instructions, resulting in an enlarged code with defects removed as the output of the Code Deformation Unit (fig. 9(b)(d)). To execute the deformation process, qubits are introduced in the appropriate state all at once, and stabilizers in the new code are measured. Importantly, this seamless integration of qubit removal and enlargement is facilitated by the unified gauge transformation perspective underlying these deformation instructions.

**Comparison with Q3DE.** As shown in fig. 7(b), Q3DE supports fixed enlargement only, whereas our Surf-Deformer allows the introduction of only the necessary number of patches to restore the code distance, resulting in savings in qubit resources needed for incorporation into the code. Moreover, the basic

---

**Algorithm 2: Adaptive Enlargement Subroutine**


---

**Input:** stabilizer set  $S$ , gauge set  $G$ ,  
defective qubit set  $D$ ,  
original code distance  $Dist$   
current code distance  $dist_X, dist_Z$

**Output:** stabilizer set  $S'$ , gauge set  $G'$

```

1 Defects =  $\emptyset$ 
2 while  $dist_X < Dist$  or  $dist_Z < Dist$  do
3   if  $dist_X < Dist$  then
4      $layer_1 = \text{find\_layer}(X_{L1})$ 
5     for  $patch \in layer_1$  do
6       if Exist  $d_i \in patch \cap D$  then
7         Find X-type  $patch_2$  that  $d_i \in patch_2$ 
8          $layer_1 = layer_1 \cup patch_2$ 
9          $D = D - d_i$ 
10        Defects = Defects +  $d_i$ 
11      end
12    end
13     $layer_2 = \text{find\_layer}(X_{L2})$ 
14    .....
15     $layer, X_L = \min(layer_1, layer_2)$ 
16    for  $patch \in layer$  do
17      PatchQ_ADD  $patch, X_L$ 
18    end
19     $dist_X = dist_X + 1$ 
20  else
21    ... similar to  $dist_Z$ 
22  end
23  for  $d_i \in Defects$  do
24    Apply algorithm 1 to remove  $d_i$ 
25  end
26 end

```

---

process in Q3DE lacks the capability to address irregular boundaries caused by defects or defects occurring on newly introduced qubits. Consequently, Q3DE may inadvertently introduce additional defective qubits during the enlargement process, leading to an increase in error sources that counteract the intended function of the introduced redundant qubits. This failure to effectively mitigate defects can result in a logical error rate that exceeds expectations.

## VI. THE LAYOUT GENERATOR

Surf-Deformer's layout generator aims to facilitate communication between surface codes in the presence of potential code enlargement due to defect mitigation. The key idea is to introduce an additional  $\Delta d$  inter-space, as shown in fig. 10(a), to accommodate enlargements of up to size  $\Delta d$  (or even  $2\Delta d$  if enlarging in both directions). The parameter  $\Delta d$  is determined by the defect error model, chosen such that enlarging within size  $\Delta d$  can effectively restore the code distance of the deformed code with high probability. Therefore, the communication channel of width  $d$  will only be compromised by code enlargement with a negligible probability.

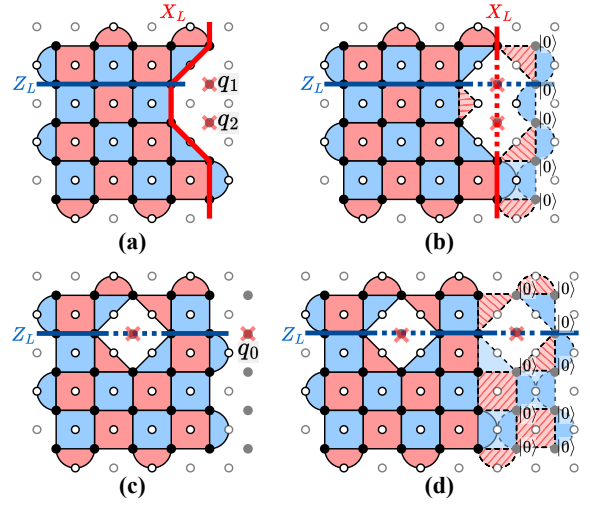


Fig. 9. Enlargement while addressing defects. (a) Removed defects create an irregular boundary. (b) Enlarging on the irregular boundary. (c) Defect can occur on prospective scale layers. (d) Enlarging by two qubit layers.

**Surf-Deformer's layout generator.** The output layout is determined by three parameters:

(1) *Logical qubit number  $N$ .* The logical qubits in the layout consist algorithmic qubits needed for the quantum program, plus the additional qubits essential for facilitating quantum computation (e.g. logical qubits prepared in magic states for implementing logical  $T$  gates [41]). These logical qubits are arranged in a lattice on a plane, with each one encoded within a surface code and equally spaced apart from one another.

(2) *Code distance  $d$ .* The code distance  $d$  should be chosen sufficiently large to maintain a sufficiently low logical error rate, ensuring that the failure rate  $\alpha_{fail}$  of the program execution remains below a certain threshold, such as 0.1%. The failure rate can be estimated based on the logical error rate and features of the quantum program, such as the number of logical gates and the space-time cost of logical gates. For further details on this estimation, please refer to [42], [60].

(3) *Additional inter-space  $\Delta d$ .* We present an error model for defects that allows us to estimate the probability of the communication channel being blocked. We assume that defects occurring on each physical qubit follow a Poisson process with rate  $\rho$ , lasting for a time  $T$ , and with a maximal size of  $D$ . Thus, the number of defects on a patch follows a Poisson distribution with parameter  $\lambda = 2d^2\rho T$ , since a surface code of code distance  $d$  contains roughly  $2d^2$  physical qubits. Therefore, the probability of having  $k$  defects on a code is  $p(k) = \frac{\lambda^k}{k!} e^{-\lambda}$ . The additional inter-space  $\Delta d$  can accommodate the enlargement for mitigating  $\lfloor \Delta d/D \rfloor$  defects without compromising the communication channel. The probability of this protection failing and the channel becoming blocked is:

$$p_{block} = 1 - \sum_{k=0}^{\lfloor \Delta d/D \rfloor} p(k) \quad (1)$$

A desired  $\Delta d$  should be chosen as the smallest value such that the block probability is below a certain threshold  $\alpha_{block}$ , such



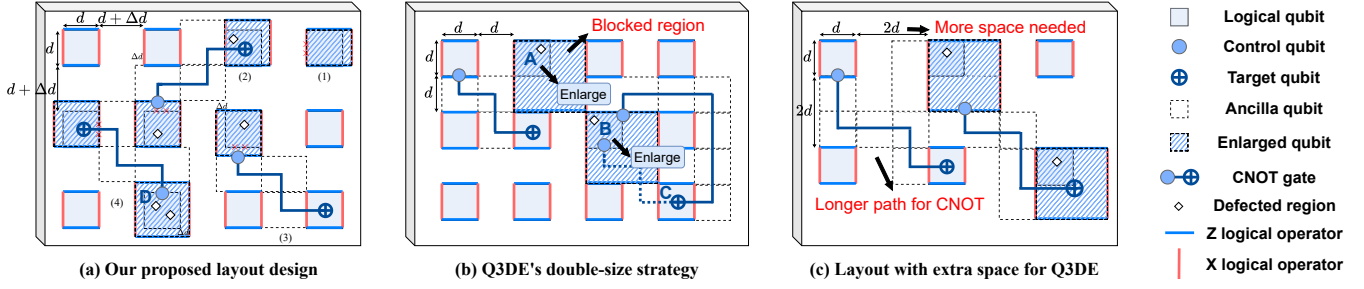


Fig. 10. (a) Our proposed layout with inter-placing width  $d + \Delta d$  can facilitate long range logical operation with lower qubit overheads while preserving code distance  $d$  of the communication channel. (b) The layout for Q3DE's double-size strategy. (c) To effectively facilitate the qubit communication in Q3DE's method, an inter-space of  $2d$  is necessary, introducing a significant qubit overhead.

as  $\alpha_{block} = 0.01$ .

For example, in experiment [22], cosmic-rays attack a 26-qubit superconducting device roughly every 10s, with each attack lasting for 25ms, and the number of affected qubits up to 24. In this case,  $\rho = 0.1\text{Hz}/26$ ,  $T = 25\text{ms}$ , and  $D \approx 4$ . For a typical surface code of size  $d = 27$  [60], its Poisson parameter is  $\lambda = 0.14$ . Here, we can choose  $\Delta d = 4$  because  $p_{block} = 1 - p(0) - p(1) \approx 0.0089 < 0.01 = \alpha_{block}$ .

**Comparison with Q3DE layout.** Q3DE's layout poses challenges on logical qubit communication due to its double-size enlargement scheme, which entirely obstructs the space between codes used for executing logical operations fig. 10(b). It has the following major limitations:

(1) *Space-time overhead of logical operations.* The blocked channel may lead to space overhead for long-distance logical operations. For example, in fig. 10(b), the CNOT gate from qubit  $B$  to  $C$  must traverse a longer path (solid line) instead of the shorter one (dotted lines) due to the enlarged qubit  $B$ . Moreover, the blocked channel can result in severe time overhead. Logical operations may become unfeasible due to blocked paths, such as the CNOT gate from qubit  $A$  to  $B$ . In such cases, the program must be paused for a long time (thousands of QEC cycles) until the effects of defects subside and the code shrinks back to its original size, making the ancilla path available again. In contrast, our layout with an extra inter-space  $\Delta d$  effectively suppresses the block probability, thus reducing the space-time cost of logical operations to a nearly optimal level.

(2) *Qubit resource for facilitating communication.* It's possible for the size-doubling strategy in Q3DE to achieve nearly optimal space and time costs, but it requires a  $2d$  inter-space (fig. 10(c)) to accommodate both code enlargement and ancilla paths of distance  $d$ . However, this results in a significant qubit resource overhead of  $(\frac{3d}{2d})^2 = 2.25$  times. In contrast, our layout introduces a lower overhead since  $\Delta d$  must be smaller than  $d$ . This overhead remains mild, especially when  $\Delta d$  is relatively small compared to the code distance  $d$ .

## VII. IMPLEMENTATION AND EVALUATION

### A. Experimental Setup

**Evaluation setting.** We use the Stim [61] stabilizer circuit simulator and the PyMatching [62] decoder for our numerical

simulations. For program compilation, we employ the lattice surgery framework described in [42], [63], along with the  $T$  factory for implementing logical  $T$  gates using magic state distillation strategies [40].

**Benchmark programs.** We have selected several quantum programs designed to tackle real-world challenges. These programs include Simon's algorithm [64], Ripple Carry Adder (RCA) [65], Quantum Fourier Transform (QFT) [66], and Grover's algorithm [5]. The first suffix of the name indicates the number of logical qubits used, while the second suffix represents the number of repetitions. For instance, "QFT-100-20" indicates the task of 20 QFT layers on 100 qubits, a common scenario used in Shor's algorithm [4].

**Metric.** For evaluation, we consider three key metrics. First, the *physical qubit count* encompasses all data and ancilla qubits used in the quantum program's layout. It quantifies the qubit resources required for the task, with lower values being preferred. Second, the *retry risk*, as defined by [60], represents the probability of an uncorrectable logical error occurring in the program, which will lead to an incorrect task result that necessitates retry. This metric indicates the error rate of task results, with lower values being preferred. Third, the *throughput* of non-local operations represents the average number of operations executed in one cycle, with higher values being preferred. This metric indicates the layout's ability to execute non-local operations (CNOT and  $T$  gates) in parallel, which can significantly impact task runtime, particularly when compared to local operations.

**Physical error model.** We employ a widely-used circuit-level error model [15], [61]. We associate same probabilities  $p = 10^{-3}$ , which is 0.1 times the surface code's error threshold, with the single-qubit depolarizing error channel for single-qubit gates, the two-qubit depolarizing error channel for two-qubit gates, and the Pauli-X error channel for measurement and reset operations.

**Dynamic defect model.** We adopt the dynamic defect model in [2], which is derived from physical experiments [22]. Each physical qubit experiences a dynamic defect event following an exponential distribution with an average event rate of  $\lambda = 1/(26 \times 10\text{ s})$  [22]. When a physical qubit is attacked, the adjacent 24 qubits are affected, resulting in a defective region

TABLE II  
RESULTS OF Q3DE , ASC-S AND SURF-DEFORMER FOR VARIOUS PROGRAMS WITH DIFFERENT SCALE

Benchmark					Q3DE		ASC-S		Surf-Deformer	
Name	# CX	# T	# qubit	$d$	# physical qubit	Retry risk	# physical qubit	Retry risk	# physical qubit	Retry risk
Simon -400-1000	$3.02 \times 10^5$	0	400	19	$1.46 \times 10^6$	OverRuntime	$1.46 \times 10^6$	53.1%	$1.80 \times 10^6$	1.51%
				21	$1.79 \times 10^6$	OverRuntime	$1.79 \times 10^6$	7.28%	$2.15 \times 10^6$	0.17%
Simon -900-1500	$1.01 \times 10^6$	0	900	21	$3.73 \times 10^6$	OverRuntime	$3.73 \times 10^6$	46.7%	$4.49 \times 10^6$	1.09%
				23	$4.47 \times 10^6$	OverRuntime	$4.47 \times 10^6$	6.14%	$5.30 \times 10^6$	0.12%
RCA -225-500	$8.96 \times 10^5$	$7.84 \times 10^5$	225	21	$1.08 \times 10^6$	OverRuntime	$1.08 \times 10^6$	41.9%	$1.30 \times 10^6$	0.98%
				23	$1.30 \times 10^6$	OverRuntime	$1.30 \times 10^6$	5.63%	$1.54 \times 10^6$	0.11%
RCA -729-100	$5.82 \times 10^5$	$5.10 \times 10^5$	729	21	$3.07 \times 10^6$	OverRuntime	$3.07 \times 10^6$	76.6%	$3.70 \times 10^6$	1.79%
				23	$3.69 \times 10^6$	OverRuntime	$3.69 \times 10^6$	10.2%	$4.37 \times 10^6$	0.20%
QFT -25-160	$1.02 \times 10^5$	$1.87 \times 10^8$	25	23	$2.39 \times 10^5$	OverRuntime	$2.39 \times 10^5$	61.4%	$2.85 \times 10^5$	1.20%
				25	$2.82 \times 10^5$	OverRuntime	$2.82 \times 10^5$	7.83%	$3.32 \times 10^5$	0.13%
QFT -100-20	$2.30 \times 10^5$	$1.58 \times 10^9$	100	25	$0.78 \times 10^6$	OverRuntime	$0.78 \times 10^6$	$\sim 100\%$	$0.92 \times 10^6$	1.69%
				27	$0.91 \times 10^6$	OverRuntime	$0.91 \times 10^6$	12.6%	$1.06 \times 10^6$	0.18%
Grover -9-80	$1.36 \times 10^5$	$1.99 \times 10^8$	9	23	$1.29 \times 10^5$	OverRuntime	$1.29 \times 10^5$	57.3%	$1.54 \times 10^5$	1.12%
				25	$1.51 \times 10^5$	OverRuntime	$1.51 \times 10^5$	7.23%	$1.79 \times 10^5$	0.12%
Grover -16-2	$4.29 \times 10^5$	$1.13 \times 10^9$	16	25	$2.12 \times 10^5$	OverRuntime	$2.12 \times 10^5$	56.0%	$2.50 \times 10^5$	0.93%
				27	$2.47 \times 10^5$	OverRuntime	$2.47 \times 10^5$	7.01%	$2.88 \times 10^5$	0.10%

of size 4. The physical error rate of qubits in the affected region increases to approximately 50% and lasts for  $T = 25$  ms, equivalent to approximately 25,000 QEC cycles [17].

### B. Overall Performance

We compare our Surf-Deformer with two previous frameworks, Q3DE method [2] and adaptive surface code (ASC-S) [33], on benchmark programs mentioned in section VII-A. The results are presented in table II. We evaluate these tasks on surface codes of appropriate distances chosen to meet the target retry risk levels of 1% and 0.1% in our framework. Overall, our Surf-Deformer in table II demonstrates a consistently better performance. In particular, we highlight the following three observations:

- 1) All tasks processed by Q3DE exhibit a retry risk of  $\sim 100\%$ , failing to mitigate the impact of dynamic defects. This limitation stems from its enlargement operation with a fixed layout, which causes the ancilla space near the defective qubits to become blocked. Additionally, the large scale of tasks necessitates high-fidelity logical qubits, implying a large code distance  $d$  for the surface code. With more qubits used to encode a logical qubit, there is a higher probability of the qubit blocks being attacked by defect events. Consequently, most qubit blocks become enlarged in Q3DE, and a significant portion of the ancilla paths are blocked. Fewer or even no available ancilla paths for executing non-local operations result in the high retry risk.
- 2) Without the ability to recover the decreased distance caused by removing defective qubits, the retry risk of tasks executed by ASC-S is 35x-70x higher than those by our Surf-Deformer. This disparity arises from the task's retry risk being determined by the worst qubit blocks during runtime, since a single logical error on any logical qubit can lead to the failure of the entire task. Failure to restore a low-distance logical qubit to the original

required distance  $d$  for the task significantly amplifies the retry risk.

- 3) With Surf-Deformer's layout, it requires only around 20% more physical qubits to resolve the communication blocking issue and achieve a low retry risk. Moreover, even with the same number of physical qubits, Surf-Deformer still outperforms ASC-S. For example, in the task "QFT-100-20," Surf-Deformer with  $d = 25$  and  $\Delta d = 4$  and ASC-S with  $d = 27$  both use roughly  $9 \times 10^5$  physical qubits. However, the retry risk of Surf-Deformer is still 6.3x lower than that of ASC-S.

### C. Analysis on Sub-components

In this section, we demonstrate the superior performance of our Surf-Deformer due to its adaptive deformation framework and layout. Our approach excels in saving qubit resources, maintaining the QEC capability of the deformed code, and enhancing surface code communication compared to other methods. We have conducted a series of experiments to showcase these advantages.

**Qubit resource saving.** We demonstrate the substantial resource savings achieved by Surf-Deformer by comparing the physical qubit count required for the layout to achieve a 1% retry risk with different methods. Our comparison includes Lattice Surgery, the revised version of Q3DE, and ASC-S. In the revised Q3DE, we adjust the inter-space to  $2d$  to prevent the enlargement from blocking surrounding communication paths, as illustrated in fig. 10(c). As depicted in fig. 12, Surf-Deformer requires significantly fewer qubits compared to all previous methods, approximately 75% less than Lattice Surgery, 50% less than Q3DE, and 15% less than ASC-S.

**Improved logical error rate by qubit removal.** In fig. 11(a), we compare the logical error rates of surface codes with and without defective qubits removed by Surf-Deformer, across different numbers of defective qubits. We didn't present the cases for  $d = 21$  and  $d = 27$  because the logical error rates are

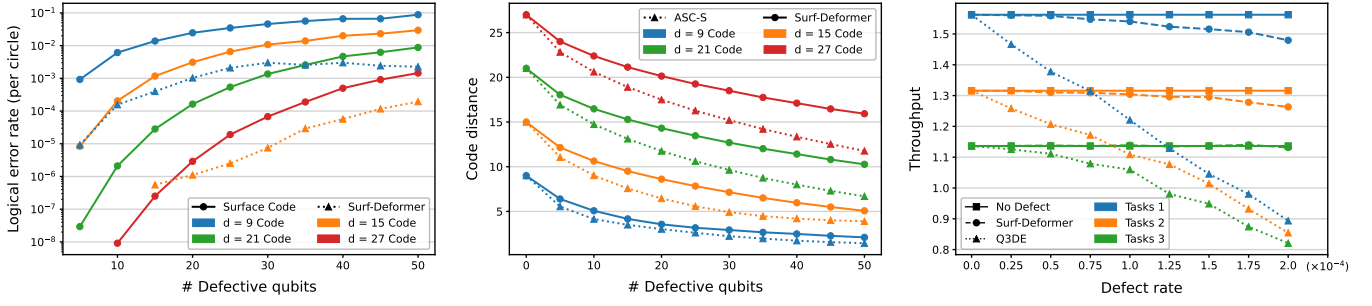


Fig. 11. (a) Logical error rates for the surface code with defect removal compared to no treatment. (b) Loss in code distance during adaptive defect removal in Surf-Deformer compared to ASC-S. (c) Throughput of quantum tasks with varying parallelism on the adaptive layout of Surf-Deformer compared to Q3DE.

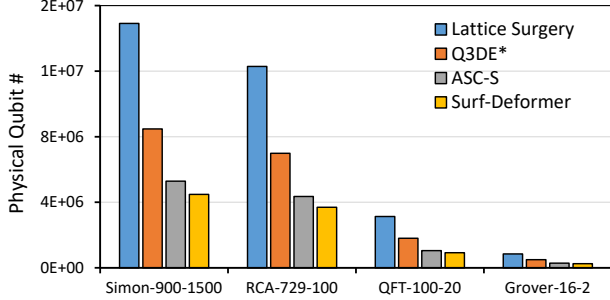


Fig. 12. Physical qubit counts required to achieve a retry risk of approximately 1%. Q3DE\* stands for the revised illustrated in fig. 10(c).

so low that numerical simulations cannot provide reasonable estimations. The results show that codes with defects removed by Surf-Deformer achieve comparable logical error rates to those without any treatment, despite having much smaller code distances. For instance, when there are 10 defective qubits, a distance-9 code with defects removed shows a similar logical error rate to a distance-15 code without any treatment. This also underscores that simply expanding the code size while retaining defective qubits, as in Q3DE, cannot effectively improve logical error rates as expected.

**Enhanced code distance by adaptive defect removal.** We compare the cost of distance recovery of Surf-Deformer and previous methods such as ASC-S that use oversimplified deformation operations. fig. 11(b) gives the code distance of defective codes of different original sizes, w.r.t. varying number of defective qubits. It indicates that our method can preserve the code distance better than the previous methods, leading to a lower cost when recovering the code distance through enlargement. Additionally, the advantage of our method becomes more significant on codes of larger size and when there are more defective qubits.

**Parallelism improvement by Surf-Deformer’s layout.** In fig. 11(c), we compare the efficiency of qubit communication using the layouts in three schemes: (1) Surf-Deformer, (2) Q3DE with  $d$  inter-space, and (3) classical lattice surgery (LS), representing optimal runtime. We consider 100 logical qubits and three sets of tasks, each comprising 5 tasks with 25 CNOT gates on 50 distinct logical qubits. The tasks in each set can be completed in 16, 19, and 22 time-steps on the

LS layout, respectively, indicating three levels of parallelism. We then sample defects 100 times for each task and compute the average throughput of each task set using the layouts in Surf-Deformer and Q3DE.

The results indicate that as the defect rate increases, the throughput significantly drops for the Q3DE layout, whereas it only experiences a slight decline with our layout. This is because expanding all the defective code to a  $2d$  size severely blocks the ancilla paths for long-range CNOT gates, resulting in a much longer execution time, while the additional  $\Delta d$  space in our layout significantly reducing the probability of ancilla paths being blocked. Therefore, the Surf-Deformer layout effectively facilitates the computation among logical qubits.

#### D. Trade-off between Qubit Resource and QEC Performance

In fig. 13(a), we compare the trade-off lines of physical qubit count and retry risk for Surf-Deformer and ASC-S. Our findings indicate that the logical error rate of logical qubits transformed by Surf-Deformer maintains the trade-off line of the non-defective surface code’s QEC performance, with the logical error rate decreasing exponentially with increasing code distance. Furthermore, Surf-Deformer demonstrates a more efficient trade-off line than ASC-S, achieving the same retry risk with lower physical qubit overhead.

Surf-Deformer’s deformation method can also be integrated with post-selection method in [33] to enhance the removal of static defects and post-selection of chiplets. As shown in fig. 13(b), Surf-Deformer’s deformation method increases the yield rate of the targeted distance-27 surface code, with more significant improvements as the size of the original patch increases. For instance, when using size-25 patches with 20 faulty qubits, the yield rate of Surf-Deformer (0.75) is approximately double that of the original ASC-S (0.39).

#### E. Robust to Various Error Models and Unreliable Detection

In this section, we evaluate Surf-Deformer’s robustness under high correlated error rates and unreliable defect detection. In fig. 14(a), we simulate and compare the logical error rates of the surface code and Surf-Deformer’s deformed code under various 2-qubit gate correlated error settings, with single-qubit error rates fixed at  $p = 0.001$ . The results show that Surf-Deformer maintains a 10x improvement over the original surface code as the correlated error rate increases. In fig. 14(b), we use an existing detection method [2] which can achieve

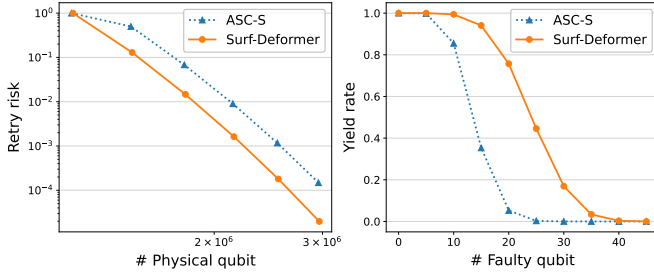


Fig. 13. (a) Trade-off between QEC performance (Retry risk) and resource efficiency (# Physical qubit) (b) Yield rates of ASC-S and Surf-Deformer for the task of deforming a  $l=35$  patch with static faulty qubits to a surface code with a distance of no less than 27.

the false-positive and true-negative detection probabilities being below 0.01. The green line, representing the unreliable detection scenario, is close to the orange line, representing the precise detection scenario, indicating that Surf-Deformer’s QEC performance remains robust even with unreliable defect detection.

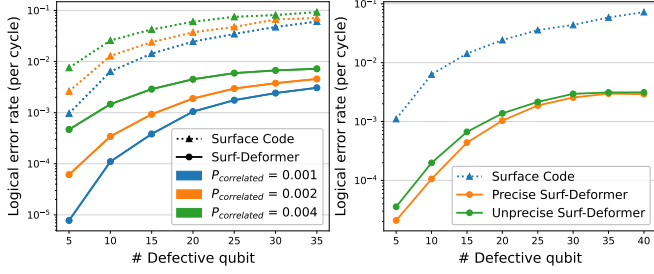


Fig. 14. Logical error rate of a distance-9 surface code under (a) various 2-qubit gates correlated errors and (b) the presence of imprecise defect detection.

## VIII. RELATED WORK

In this section, we present a broader perspective on approaches for addressing dynamic defects in quantum hardware. Generally, there are three main directions to consider:

**(1) Hardware-level solutions.** Dynamic defects can be mitigated at the hardware level to reduce their incidence rate. Physical techniques such as shielding [24], [30], phonon downconversion [67], [68], and metallic covers [69] can help mitigate the burst of quasiparticles induced by radiation materials and cosmic rays, which is a main source of qubit decoherence. Various mitigation methods on chips [21], [70], [71] are also proposed. However, although these hardware-level solutions can improve the defect rate of physical qubit, it is often insufficient for meaningful quantum computations, which can take several hours [60], to be effectively executed at low retry risk. Although preventing these defects at the hardware level is challenging, specialized hardware detectors [31], [32] can often locate them accurately at runtime with statistical methods.

**(2) Software-level solution.** To address dynamic defects that involve varying error rates, methods like [2], [72], [73], [74] estimate modified error rates based on historical syndrome data

and then adjust the error rates in the decoders such as MWPM [47], [48], [75], [76], [77], [78]. Various error mitigation approaches [79], [80], [81] based on statistical methods are also proposed. However, these methods become ineffective when the physical error rate is considerably high or the errors can propagate, but these are often the case with dynamic defects, where defected qubits can have error rates near 50% and affect the integrity of adjacent qubits [22], [25].

**(3) QEC-level solution.** Theoretical frameworks have been established for converting one stabilizer code to another [52], [57], [82], [83], [84] by modifying the code through a series of measurements. However, these methods either potentially modify the encoded information [52], [84], or ignore the hardware constraints on qubit connectivity [57], limiting their code conversion procedure for practical use. On the other hand, approaches such as [1], [2], [50] design new codes based on the structure of the underlying hardware. However, these methods are inefficient in utilizing the remaining intact qubits, do not detail the specific deformation procedure, and overlook the feasibility of communication between logical qubits.

## IX. CONCLUSION

We introduce Surf-Deformer, a novel deformation framework that expands the surface code instruction set to integrate adaptive defect mitigation functionalities. With four meticulously designed deformation instructions, Surf-Deformer creates a larger design space, enabling optimized deformation processes tailored to specific defects. Combined with a new adaptive code layout, Surf-Deformer enhances qubit communication efficiency and reduces logical error rates with minimal additional qubit resources. Comprehensive evaluations show that Surf-Deformer produces deformed codes with superior QEC capabilities and more efficient qubit communication. Surf-Deformer is a versatile tool for effectively addressing defects in surface codes across various quantum platforms.

## ACKNOWLEDGMENT

We thank the anonymous reviewers for their constructive feedback and AWS Cloud Credit for Research. This work is supported in part by Robert N. Noyce Trust, NSF 2048144, NSF 2422169, NSF 2427109. This material is based upon work supported by the U.S. Department of Energy, Office of Science, National Quantum Information Science Research Centers, Quantum Science Center. This research used resources of the Oak Ridge Leadership Computing Facility, which is a DOE Office of Science User Facility supported under Contract DE-AC05-00OR22725. The Pacific Northwest National Laboratory is operated by Battelle for the U.S. Department of Energy under Contract DE-AC05-76RL01830.

## REFERENCES

- [1] Adam Siegel, Armands Strikis, Thomas Flatters, and Simon Benjamin. Adaptive surface code for quantum error correction in the presence of temporary or permanent defects. *Quantum*, 7:1065, 2023.
- [2] Yasunari Suzuki, Takanori Sugiyama, Tomochika Arai, Wang Liao, Koji Inoue, and Teruo Tanimoto. Q3de: A fault-tolerant quantum computer architecture for multi-bit burst errors by cosmic rays. In *2022 55th IEEE/ACM International Symposium on Microarchitecture (MICRO)*, pages 1110–1125. IEEE, 2022.



- [3] John Preskill. Quantum computing in the nisy era and beyond. *Quantum*, 2:79, 2018.
- [4] Peter W Shor. Polynomial-time algorithms for prime factorization and discrete logarithms on a quantum computer. *SIAM review*, 41(2):303–332, 1999.
- [5] Lov K Grover. A fast quantum mechanical algorithm for database search. In *Proceedings of the twenty-eighth annual ACM symposium on Theory of computing*, pages 212–219, 1996.
- [6] Alberto Peruzzo, Jarrod McClean, Peter Shadbolt, Man-Hong Yung, Xiao-Qi Zhou, Peter J Love, Alán Aspuru-Guzik, and Jeremy L O’Brien. A variational eigenvalue solver on a photonic quantum processor. *Nature communications*, 5(1):4213, 2014.
- [7] Peter W Shor. Fault-tolerant quantum computation. In *Proceedings of 37th conference on foundations of computer science*, pages 56–65. IEEE, 1996.
- [8] A Robert Calderbank and Peter W Shor. Good quantum error-correcting codes exist. *Physical Review A*, 54(2):1098, 1996.
- [9] Andrew Steane. Multiple-particle interference and quantum error correction. *Proceedings of the Royal Society of London. Series A: Mathematical, Physical and Engineering Sciences*, 452(1954):2551–2577, 1996.
- [10] Sergey B Bravyi and A Yu Kitaev. Quantum codes on a lattice with boundary. *arXiv preprint quant-ph/9811052*, 1998.
- [11] Héctor Bombín and Miguel A Martin-Delgado. Optimal resources for topological two-dimensional stabilizer codes: Comparative study. *Physical Review A*, 76(1):012305, 2007.
- [12] Hector Bombin and Miguel Angel Martin-Delgado. Topological quantum distillation. *Physical review letters*, 97(18):180501, 2006.
- [13] Peter W Shor. Scheme for reducing decoherence in quantum computer memory. *Physical review A*, 52(4):R2493, 1995.
- [14] A Yu Kitaev. Fault-tolerant quantum computation by anyons. *Annals of physics*, 303(1):2–30, 2003.
- [15] Austin G Fowler, Matteo Mariantoni, John M Martinis, and Andrew N Cleland. Surface codes: Towards practical large-scale quantum computation. *Physical Review A*, 86(3):032324, 2012.
- [16] Simon J Devitt, William J Munro, and Kae Nemoto. Quantum error correction for beginners. *Reports on Progress in Physics*, 76(7):076001, 2013.
- [17] Suppressing quantum errors by scaling a surface code logical qubit. *Nature*, 614(7949):676–681, 2023.
- [18] Youwei Zhao, Yangsen Ye, He-Liang Huang, Yiming Zhang, Dachao Wu, Huijie Guan, Qingling Zhu, Zuolin Wei, Tan He, Sirui Cao, et al. Realization of an error-correcting surface code with superconducting qubits. *Physical Review Letters*, 129(3):030501, 2022.
- [19] Dolev Bluvstein, Simon J Evered, Alexandra A Geim, Sophie H Li, Hengyun Zhou, Tom Manovitz, Sepehr Ebadi, Madelyn Cain, Marcin Kalinowski, Dominik Hangleiter, et al. Logical quantum processor based on reconfigurable atom arrays. *Nature*, 626(7997):58–65, 2024.
- [20] Sebastian Krinner, Nathan Lacroix, Ants Remm, Agustin Di Paolo, Elie Genois, Catherine Leroux, Christoph Hellings, Stefania Lazar, Francois Swadek, Johannes Herrmann, et al. Realizing repeated quantum error correction in a distance-three surface code. *Nature*, 605(7911):669–674, 2022.
- [21] John M Martinis. Saving superconducting quantum processors from decay and correlated errors generated by gamma and cosmic rays. *npj Quantum Information*, 7(1):90, 2021.
- [22] Matt McEwen, Lara Faoro, Kunal Arya, Andrew Dunsworth, Trent Huang, Seon Kim, Brian Burkett, Austin Fowler, Frank Arute, Joseph C Bardin, et al. Resolving catastrophic error bursts from cosmic rays in large arrays of superconducting qubits. *Nature Physics*, 18(1):107–111, 2022.
- [23] Christopher D Wilen, S Abdullah, NA Kurinsky, C Stanford, L Cardani, G d’Imperio, C Tomei, L Faoro, LB Ioffe, CH Liu, et al. Correlated charge noise and relaxation errors in superconducting qubits. *Nature*, 594(7863):369–373, 2021.
- [24] Antti P Vepsäläinen, Amir H Karamlou, John L Orrell, Akshunna S Dogra, Ben Loer, Francisca Vasconcelos, David K Kim, Alexander J Melville, Bethany M Niedzielski, Jonilyn L Yoder, et al. Impact of ionizing radiation on superconducting qubit coherence. *Nature*, 584(7822):551–556, 2020.
- [25] Natalie C Brown, Michael Newman, and Kenneth R Brown. Handling leakage with subsystem codes. *New Journal of Physics*, 21(7):073055, 2019.
- [26] Iris Cong, Harry Levine, Alexander Keesling, Dolev Bluvstein, Sheng-Tao Wang, and Mikhail D. Lukin. Hardware-efficient, fault-tolerant quantum computation with rydberg atoms, 2022.
- [27] E Gümüş, Danial Majidi, Danilo Nikolić, Patrick Raif, Bayan Karimi, Joonas T Peltonen, Elke Scheer, Jukka P Pekola, Hervé Courtois, Wolfgang Belzig, et al. Calorimetry of a phase slip in a josephson junction. *Nature Physics*, 19(2):196–200, 2023.
- [28] Matthew L Day, Pei Jiang Low, Brendan White, Rajibul Islam, and Crystal Senko. Limits on atomic qubit control from laser noise. *npj Quantum Information*, 8(1):72, 2022.
- [29] Jonathan J Burnett, Andreas Bengtsson, Marco Scigliuzzo, David Niepc, Marina Kudra, Per Delsing, and Jonas Bylander. Decoherence benchmarking of superconducting qubits. *npj Quantum Information*, 5(1):54, 2019.
- [30] Laura Cardani, Francesco Valenti, Nicola Casali, Gianluigi Catelani, Thibault Charpentier, Massimiliano Clemenza, Ivan Colantoni, Angelo Cruciani, G D’Imperio, Luca Gironi, et al. Reducing the impact of radioactivity on quantum circuits in a deep-underground facility. *Nature communications*, 12(1):2733, 2021.
- [31] James T Farmer, Azarin Zarassi, Darian M Hartsell, Evangelos Vlachos, Haimeng Zhang, and Eli M Levenson-Falk. Continuous real-time detection of quasiparticle trapping in aluminum nanobridge josephson junctions. *Applied Physics Letters*, 119(12), 2021.
- [32] Willemijn Uilhoorn, James G Kroll, Arno Bargerbos, Syed D Nabi, Chung-Kai Yang, Peter Krogstrup, Leo P Kouwenhoven, Angela Kou, and Gijs de Lange. Quasiparticle trapping by orbital effect in a hybrid superconducting-semiconducting circuit. *arXiv preprint arXiv:2105.11038*, 2021.
- [33] Sophia Fuhui Lin, Joshua Viszlai, Kaitlin N Smith, Gokul Subramanian Ravi, Charles Yuan, Frederic T Chong, and Benjamin J Brown. Codesign of quantum error-correcting codes and modular chiplets in the presence of defects. In *Proceedings of the 29th ACM International Conference on Architectural Support for Programming Languages and Operating Systems, Volume 2*, pages 216–231, 2024.
- [34] Kaitlin N Smith, Gokul Subramanian Ravi, Jonathan M Baker, and Frederic T Chong. Scaling superconducting quantum computers with chiplet architectures. In *2022 55th IEEE/ACM International Symposium on Microarchitecture (MICRO)*, pages 1092–1109. IEEE, 2022.
- [35] Thomas M Stace, Sean D Barrett, and Andrew C Doherty. Thresholds for topological codes in the presence of loss. *Physical review letters*, 102(20):200501, 2009.
- [36] Thomas M Stace and Sean D Barrett. Error correction and degeneracy in surface codes suffering loss. *Physical Review A*, 81(2):022317, 2010.
- [37] James M Auger, Hussain Anwar, Mercedes Gimeno-Segovia, Thomas M Stace, and Dan E Browne. Fault-tolerance thresholds for the surface code with fabrication errors. *Physical Review A*, 96(4):042316, 2017.
- [38] Shota Nagayama, Austin G Fowler, Dominic Horsman, Simon J Devitt, and Rodney Van Meter. Surface code error correction on a defective lattice. *New Journal of Physics*, 19(2):023050, 2017.
- [39] Dominic Horsman, Austin G Fowler, Simon Devitt, and Rodney Van Meter. Surface code quantum computing by lattice surgery. *New Journal of Physics*, 14(12):123011, 2012.
- [40] Austin G Fowler and Craig Gidney. Low overhead quantum computation using lattice surgery. *arXiv preprint arXiv:1808.06709*, 2018.
- [41] Michael Beverland, Vadym Kliuchnikov, and Eddie Schoute. Surface code compilation via edge-disjoint paths. *PRX Quantum*, 3(2):020342, 2022.
- [42] Daniel Litinski. A game of surface codes: Large-scale quantum computing with lattice surgery. *Quantum*, 3:128, 2019.
- [43] Tyler LeBlond, Ryan S Bennink, Justin G Lietz, and Christopher M Seck. Tisc: A surface code compiler and resource estimator for trapped-ion processors. In *Proceedings of the SC’23 Workshops of The International Conference on High Performance Computing, Network, Storage, and Analysis*, pages 1426–1435, 2023.
- [44] Michael A Nielsen and Isaac L Chuang. *Quantum computation and quantum information*. Cambridge university press, 2010.
- [45] Daniel Gottesman. Class of quantum error-correcting codes saturating the quantum hamming bound. *Physical Review A*, 54(3):1862, 1996.
- [46] Daniel Gottesman. The heisenberg representation of quantum computers, 1998.
- [47] Eric Dennis, Alexei Kitaev, Andrew Landahl, and John Preskill. Topological quantum memory. *Journal of Mathematical Physics*, 43(9):4452–4505, 2002.

- [48] Austin G Fowler. Optimal complexity correction of correlated errors in the surface code. *arXiv preprint arXiv:1310.0863*, 2013.
- [49] Naomi H Nickerson and Benjamin J Brown. Analysing correlated noise on the surface code using adaptive decoding algorithms. *Quantum*, 3:131, 2019.
- [50] Armands Strikis, Simon C Benjamin, and Benjamin J Brown. Quantum computing is scalable on a planar array of qubits with fabrication defects. *Physical Review Applied*, 19(6):064081, 2023.
- [51] Jiri Vala, K Birgitta Whaley, and David S Weiss. Quantum error correction of a qubit loss in an addressable atomic system. *Physical Review A*, 72(5):052318, 2005.
- [52] Christophe Vuillot, Lingling Lao, Ben Criger, Carmen García Almudéver, Koen Bertels, and Barbara M Terhal. Code deformation and lattice surgery are gauge fixing. *New Journal of Physics*, 21(3):033028, 2019.
- [53] David Poulin. Stabilizer formalism for operator quantum error correction. *Physical review letters*, 95(23):230504, 2005.
- [54] Sergey Bravyi, Guillaume Duclos-Cianci, David Poulin, and Martin Suchara. Subsystem surface codes with three-qubit check operators. *arXiv preprint arXiv:1207.1443*, 2012.
- [55] Dave Bacon. Operator quantum error-correcting subsystems for self-correcting quantum memories. *Physical Review A*, 73(1):012340, 2006.
- [56] David W Kribs, Raymond Laflamme, David Poulin, and Maia Lesosky. Operator quantum error correction. *arXiv preprint quant-ph/0504189*, 2005.
- [57] Kristina R Colladay and Erich J Mueller. Rewiring stabilizer codes. *New Journal of Physics*, 20(8):083030, 2018.
- [58] Keyi Yin, Hezi Zhang, Yunong Shi, Travis Humble, Ang Li, and Yufei Ding. Surf-deformer: Mitigating dynamic defects on surface code via adaptive deformation. *arXiv preprint arXiv:2405.06941*, 2024.
- [59] Avimta Chatterjee, Subrata Das, and Swaroop Ghosh. Lattice surgery for dummies. *arXiv preprint arXiv:2404.13202*, 2024.
- [60] Craig Gidney and Martin Ekerå. How to factor 2048 bit rsa integers in 8 hours using 20 million noisy qubits. *Quantum*, 5:433, 2021.
- [61] Craig Gidney. Stim: a fast stabilizer circuit simulator. *Quantum*, 5:497, 2021.
- [62] Oscar Higgott. Pymatching: A python package for decoding quantum codes with minimum-weight perfect matching. *ACM Transactions on Quantum Computing*, 3(3):1–16, 2022.
- [63] George Watkins, Hoang Minh Nguyen, Varun Seshadri, Keelan Watkins, Steven Pearce, Hoi-Kwan Lau, and Alexandru Paler. A high performance compiler for very large scale surface code computations. *arXiv preprint arXiv:2302.02459*, 2023.
- [64] Daniel R Simon. On the power of quantum computation. *SIAM journal on computing*, 26(5):1474–1483, 1997.
- [65] Yasuhiro Takahashi and Noboru Kunihiro. A linear-size quantum circuit for addition with no ancillary qubits. *Quantum Information & Computation*, 5(6):440–448, 2005.
- [66] Don Coppersmith. An approximate fourier transform useful in quantum factoring. *arXiv preprint quant-ph/0201067*, 2002.
- [67] K Karatsu, A Endo, J Bueno, PJ De Visser, R Barends, DJ Thoen, V Murugesan, N Tomita, and JJA Baselmans. Mitigation of cosmic ray effect on microwave kinetic inductance detector arrays. *Applied Physics Letters*, 114(3), 2019.
- [68] V Iqbal, J Ku, A Ballard, CP Larson, E Yelton, CH Liu, S Patel, R McDermott, and BLT Plourde. Phonon downconversion to suppress correlated errors in superconducting qubits. *Nature Communications*, 13(1):6425, 2022.
- [69] Xianchuan Pan, Yuxuan Zhou, Haolan Yuan, Lifu Nie, Weiwei Wei, Libo Zhang, Jian Li, Song Liu, Zhi Hao Jiang, Gianluigi Catelani, et al. Engineering superconducting qubits to reduce quasiparticles and charge noise. *Nature Communications*, 13(1):7196, 2022.
- [70] Matt McEwen, Dvir Kafri, Z Chen, Juan Atalaya, KJ Satzinger, Chris Quintana, Paul Victor Klimov, Daniel Sank, C Gidney, AG Fowler, et al. Removing leakage-induced correlated errors in superconducting quantum error correction. *Nature communications*, 12(1):1761, 2021.
- [71] Matt McEwen, Kevin C Miao, Juan Atalaya, Alex Bilmes, Alex Crook, Jenna Bovaird, John Mark Kreikebaum, Nicholas Zobrist, Evan Jeffrey, Bicheng Ying, et al. Resisting high-energy impact events through gap engineering in superconducting qubit arrays. *arXiv preprint arXiv:2402.15644*, 2024.
- [72] Josu Etxezarreta Martinez, Patricio Fuentes, Pedro Crespo, and Javier Garcia-Frias. Time-varying quantum channel models for superconducting qubits. *npj Quantum Information*, 7(1):115, 2021.
- [73] Oscar Higgott, Thomas C Bohdanowicz, Aleksander Kubica, Steven T Flammia, and Earl T Campbell. Improved decoding of circuit noise and fragile boundaries of tailored surface codes. *Physical Review X*, 13(3):031007, 2023.
- [74] Austin G Fowler, D Sank, J Kelly, R Barends, and John M Martinis. Scalable extraction of error models from the output of error detection circuits. *arXiv preprint arXiv:1405.1454*, 2014.
- [75] Austin G Fowler, Adam C Whiteside, and Lloyd CL Hollenberg. Towards practical classical processing for the surface code. *Physical review letters*, 108(18):180501, 2012.
- [76] Oscar Higgott and Craig Gidney. Sparse blossom: correcting a million errors per core second with minimum-weight matching, 2023.
- [77] Nicolas Delfosse and Jean-Pierre Tillich. A decoding algorithm for css codes using the x/z correlations. In *2014 IEEE International Symposium on Information Theory*, pages 1071–1075. IEEE, 2014.
- [78] Hanrui Wang, Pengyu Liu, Yilian Liu, Jiaqi Gu, Jonathan Baker, Frederic T. Chong, and Song Han. Dgr: Tackling drifted and correlated noise in quantum error correction via decoding graph re-weighting, 2023.
- [79] Christophe Piveteau, David Sutter, Sergey Bravyi, Jay M Gambetta, and Kristan Temme. Error mitigation for universal gates on encoded qubits. *Physical review letters*, 127(20):200505, 2021.
- [80] Kristan Temme, Sergey Bravyi, and Jay M Gambetta. Error mitigation for short-depth quantum circuits. *Physical review letters*, 119(18):180509, 2017.
- [81] Sergey Bravyi, Sarah Sheldon, Abhinav Kandala, David C Mckay, and Jay M Gambetta. Mitigating measurement errors in multiqubit experiments. *Physical Review A*, 103(4):042605, 2021.
- [82] Charles D Hill, Austin G Fowler, David S Wang, and Lloyd CL Hollenberg. Fault-tolerant quantum error correction code conversion. *Quantum Information & Computation*, 13(5-6):439–451, 2013.
- [83] Yongsoo Hwang, Byung-Soo Choi, Young-chai Ko, and Jun Heo. Fault-tolerant conversion between stabilizer codes by clifford operations. *arXiv preprint arXiv:1511.02596*, 2015.
- [84] Héctor Bombín and Miguel Angel Martin-Delgado. Quantum measurements and gates by code deformation. *Journal of Physics A: Mathematical and Theoretical*, 42(9):095302, 2009.

## A. Proofs for the logical state preservation

In this appendix, we prove that the gauge transformation does not alter the logical state stored in the subsystem stabilizer code. Based on the stabilizer formalism [53], a  $[n, k]$  subsystem stabilizer code  $\mathbb{C}$ , which encodes  $n$  physical qubits into  $k$  logical qubits, can always be represented as:

$$s_1, \dots, s_{n-k-l}, \begin{bmatrix} \bar{X}_1 \\ \bar{Z}_1 \end{bmatrix}, \dots, \begin{bmatrix} \bar{X}_k \\ \bar{Z}_k \end{bmatrix}, \begin{bmatrix} \bar{X}_{k+1} \\ \bar{Z}_{k+1} \end{bmatrix}, \dots, \begin{bmatrix} \bar{X}_{k+l} \\ \bar{Z}_{k+l} \end{bmatrix}$$

where  $s$ ,  $\bar{X}$ , and  $\bar{Z}$  are length- $n$  Pauli strings representing the operators acting on the  $n$  physical qubits. The operators  $s_1, \dots, s_{n-k-l}$  are the stabilizer generators of the code  $\mathbb{C}$ .  $\bar{X}_i$  and  $\bar{Z}_i$  represent the logical  $X$  and  $Z$  operators for the  $i$ -th logical qubit. Similarly,  $\bar{X}_{k+i}$  and  $\bar{Z}_{k+i}$  correspond to the logical  $X$  and  $Z$  operators for the  $i$ -th gauge qubit, indicating that this degree of freedom is not used to store information. We refer to this as the *generator representation* of code  $\mathbb{C}$ . For example, the original surface code has  $k = 1$  and  $l = 0$ . From the theory of stabilizer formalism, we have:

**Theorem 1.** *A generator representation is valid for a code  $\mathbb{C}$  if and only if it satisfies the following conditions:*

- (1) *All operators are independent, meaning that the product of any subset of the operator set  $\{s\} \cup \{\bar{X}\} \cup \{\bar{Z}\}$  does not equal to the identity operator  $\mathbb{I}$ .*
- (2) *The two logical operators on a single logical qubit or gauge qubit must anti-commute:  $\bar{X}_i \bar{Z}_i = -\bar{Z}_i \bar{X}_i$ .*
- (3) *Apart from the operator pairs in (2), any two operators in  $\{s\} \cup \{\bar{X}\} \cup \{\bar{Z}\}$  must commute.*

Without loss of generality, let us consider the case  $k = 1$  in the following part, which corresponds to the surface code setting used in our Surf-Deformer. The case for  $k > 1$  can be proven in a similar manner. The generator representation of a  $k = 1$  code  $\mathbb{C}$  is:

$$s_1, \dots, s_{n-l-1}, \begin{bmatrix} \bar{X}_L \\ \bar{Z}_L \end{bmatrix}, \begin{bmatrix} \bar{X}_1 \\ \bar{Z}_1 \end{bmatrix}, \dots, \begin{bmatrix} \bar{X}_l \\ \bar{Z}_l \end{bmatrix}$$

For any code state  $|\psi\rangle$  in the code space  $\mathbb{C}$ , it can always be represent as:

$$|\psi\rangle = \alpha|\psi_0\rangle + \beta|\psi_1\rangle$$

where  $|\psi_0\rangle$  and  $|\psi_1\rangle$  are the logical zero and one state identified by  $\bar{Z}_L$ :

$$\bar{Z}_L|\psi_0\rangle = |\psi_0\rangle, \quad \bar{Z}_L|\psi_1\rangle = -|\psi_1\rangle$$

Then we have the definition of logical state preservation:

**Definition 2.** *When a code  $\mathbb{C}$  is deformed to  $\mathbb{C}'$ , the deformation process is said to be logical-state-preserving on  $\bar{Z}_L$  if and only if, for any code state  $|\psi\rangle$  in  $\mathbb{C}$ , the resulting state after deformation remains  $|\psi'\rangle = \alpha|\psi'_0\rangle + \beta|\psi'_1\rangle$ , where  $|\psi'_0\rangle$  and  $|\psi'_1\rangle$  are the logical zero and one states identified by the new logical operator  $\bar{Z}'_L$  of the code  $\mathbb{C}'$ .*

**Definition 3.** *When a code  $\mathbb{C}$  is deformed to  $\mathbb{C}'$ , the deformation process is said to be logical-state-preserving if and only if it is logical-state-preserving on both  $\bar{X}_L$  and  $\bar{Z}_L$ .*

It is important to note that the generator representation of a code  $\mathbb{C}$  is not identical to the stabilizers and gauge operators measured in practice. The set of operators actually measured by the circuit can be expressed as  $Meas = Stab \cup Gauge$ . The stabilizer set  $Stab$  is measured in every cycle, while

To determine whether a code  $\mathbb{C}$  can get all necessary error syndromes by measuring  $Meas$ , we define the validity of  $Meas$ :

**Definition 4.** *A operator set  $Meas$  is valid for a code  $\mathbb{C}$  if and only if it satisfies the following conditions:*

- (1)  $Stab \subseteq \langle s_1, \dots, s_{n-l-1} \rangle$
- (2)  $Gauge \subseteq \langle s_1, \dots, s_{n-l-1}, \bar{X}_1, \bar{Z}_1, \dots, \bar{X}_l, \bar{Z}_l \rangle \setminus \langle s_1, \dots, s_{n-l-1} \rangle$
- (3)  $\{s_1, \dots, s_{n-k-1}\} \subseteq \langle Meas \rangle$

For example, a trivial measurement set for the code  $\mathbb{C}$  is  $Stab = \{s_1, \dots, s_{n-k-1}\}$  and  $Gauge = \emptyset$ . Conditions 1 and 2 ensure that the measured stabilizers and gauge operators are generated from sets that exclude the logical operators  $X_L$  and  $Z_L$  on the logical qubit. As a result, measuring the operators in  $Stab$  and  $Gauge$  will not affect the logical state within the valid code space of  $\mathbb{C}$ , which is a fundamental property of the subsystem stabilizer code [53].

Condition 3 ensures that the error syndrome for each stabilizer generator  $s_i$  can be determined from the measurement results of  $Stab$  and  $Gauge$ . For example, in fig. 6(a), the super-stabilizers  $s_1 s_2$  and  $g_1 g_2$  are two stabilizer generators in the deformed code  $\mathbb{C}'$ , and their results can be inferred from  $Gauge = \{s'_1, s'_2, g'_1, g'_2\}$ , as  $s_1 s_2 = s'_1 s'_2$  and  $g_1 g_2 = g'_1 g'_2$ .

In the following, we discuss the four types of gauge transformations formalized in II and demonstrate how each preserves the logical state:

**Stabilizer-to-Stabilizer (S2S) Transformation:** The S2S transformation identifies two stabilizers,  $\hat{s}_i, \hat{s}_j \in Stab$ , and either replaces one of them with  $\hat{s}_i \hat{s}_j$  or adds  $\hat{s}_i \hat{s}_j$  to the  $Stab$ . This transformation does not alter the generator representation of the code  $\mathbb{C}$ . The updated measurement set,  $Meas'$ , remains valid for the code  $\mathbb{C}$ , since the transformation does not change the generated group, which means  $\langle Meas \rangle = \langle Meas' \rangle$ . Therefore, measuring the new  $Meas'$  will not disturb the logical state.

**Gauge-to-Gauge (G2G) Transformation:** The G2G transformation identifies a gauge operator,  $\hat{g} \in Gauge$ , and a measurement operator,  $\hat{m} \in Meas$ . If  $\hat{g}\hat{m} \notin \langle s_1, \dots, s_{n-l-1} \rangle$ , the transformation either replaces  $\hat{g}$  with  $\hat{g}\hat{m}$  or adds  $\hat{g}\hat{m}$  to  $Gauge$ . Like S2S transformation, G2G transformation will not alter the generator representation of the code  $\mathbb{C}$  and disturb the logical state.

**Stabilizer-to-Gauge (S2G) Transformation:** The S2G transformation identifies a new operator  $\hat{g}$  and all the stabilizers that anti-commute with it:

$$Anti = \{\hat{s}_i \in Stab \mid \hat{g}\hat{s}_i = -\hat{s}_i\hat{g}\}$$

If  $Anti \neq \emptyset$ , this transformation adds  $\hat{g}$  to  $Gauge$  and moves elements of  $Anti$  from  $Stab$  to  $Gauge$ . It follows that  $Meas' = Meas \cup \{g\}$ , meaning the only practical change is the measurement of the new gauge operator  $\hat{g}$ .

To illustrate how the code  $\mathbb{C}$  is deformed, let us first provide an equivalent generator representation for the code  $\mathbb{C}$ .

**Theorem 5.** *For any code  $\mathbb{C}$  and any new operator  $g$ , if there exists a stabilizer generator  $s_k$  that anti-commutes with  $g$ , there is an alternative generator representation of the code  $\mathbb{C}$ :*

$$s'_1, \dots, s_k, \dots, s'_{n-l-1}, \begin{bmatrix} \bar{X}'_L \\ \bar{Z}'_L \end{bmatrix}, \begin{bmatrix} \bar{X}'_1 \\ \bar{Z}'_1 \end{bmatrix}, \dots, \begin{bmatrix} \bar{X}'_l \\ \bar{Z}'_l \end{bmatrix}$$

where  $g$  commutes with all operators in the set  $\{s'\} \cup \{\bar{X}'\} \cup \{\bar{Z}'\}$ .

**Proof:** If  $s_i \neq s_k$  anti-commutes with  $g$ , define  $s'_i = s_k s_i$ . Similarly, if  $\bar{X}_i$  (or  $\bar{Z}_i$ ) anti-commutes with  $g$ , define  $\bar{X}'_i = s_k \bar{X}_i$  (or  $\bar{Z}'_i = s_k \bar{Z}_i$ ). Since this replacement does not alter the generated stabilizer group, logical operator group, or gauge operator group, it provides an alternative generator representation for the code  $\mathbb{C}$ , where only  $s_k$  anti-commutes with  $g$ .

For  $Anti \neq \emptyset$ , we can always find a stabilizer generator  $s_i$  that anti-commutes with the new gauge operator  $\hat{g}$ . This is because any stabilizer  $\hat{s}$  in  $Anti$  can be expressed as a product of stabilizer generators, and at least one of these generators must anti-commute with  $\hat{g}$ .

**Theorem 6.** *While preserving the logical state of code  $\mathbb{C}$ , the S2G transformation with new gauge operator  $g$  deforms it into a new code  $\mathbb{C}'$ :*

$$s'_1, \dots, \begin{bmatrix} s_k \\ g \end{bmatrix}, \dots, s'_{n-l-1}, \begin{bmatrix} \bar{X}'_L \\ \bar{Z}'_L \end{bmatrix}, \begin{bmatrix} \bar{X}'_1 \\ \bar{Z}'_1 \end{bmatrix}, \dots, \begin{bmatrix} \bar{X}'_l \\ \bar{Z}'_l \end{bmatrix}$$

which only replace stabilizer generator  $s_i$  with a pair of gauge operators  $(s_k, g)$ .

**Proof:** For any code state  $|\psi\rangle = \alpha|\psi_0\rangle + \beta|\psi_1\rangle$ , we can denote:

$$\begin{aligned} |\psi_0\rangle &= \frac{|\psi_0\rangle + g|\psi_0\rangle}{2} + \frac{|\psi_0\rangle - g|\psi_0\rangle}{2} := \frac{|P_0\rangle}{\sqrt{2}} + \frac{|N_0\rangle}{\sqrt{2}} \\ |\psi_1\rangle &= \frac{|\psi_1\rangle + g|\psi_1\rangle}{2} + \frac{|\psi_1\rangle - g|\psi_1\rangle}{2} := \frac{|P_1\rangle}{\sqrt{2}} + \frac{|N_1\rangle}{\sqrt{2}} \end{aligned}$$

since  $s_k|P_{0/1}\rangle = |N_{0/1}\rangle$ . It is easy to see that

$$\begin{aligned} g|P_{0/1}\rangle &= |P_{0/1}\rangle, \\ g|N_{0/1}\rangle &= -|N_{0/1}\rangle. \end{aligned}$$

Thus, after measurement of  $g$ , the resulting state will be  $|\psi'\rangle = \alpha|P_0\rangle + \beta|P_1\rangle$  if the measurement result is 0, or  $|\psi'\rangle = \alpha|N_0\rangle + \beta|N_1\rangle$  if the measurement result is 1.

Since  $g$  commutes with the logical operator  $\bar{Z}'_L$ , the states  $|P_0\rangle$  and  $|N_0\rangle$  correspond to the logical zero state identified by  $\bar{Z}'_L$ , while  $|P_1\rangle$  and  $|N_1\rangle$  correspond to the logical one state.

The proof for  $X_L$  can be derived in a similar manner. Therefore, the process of S2G transformation is logical-state-preserving.

**Gauge-to-Stabilizer (G2S) Transformation:** The G2G transformation identifies a gauge operator  $\hat{g} \in Gauge$  and all gauge operators that anti-commute with it:

$$Anti = \{\hat{g}_i \in Gauge \mid \hat{g}\hat{g}_i = -\hat{g}_i\hat{g}\}$$

If  $|Anti| > 1$ , perform additional G2G transformations until  $|Anti| = 1$ . This ensures that the measurement set  $Meas'$  remains valid for the deformed code  $\mathbb{C}'$ . Finally, this transformation adds  $\hat{g}$  to the stabilizer set  $Stab$  and removes the elements of  $Anti$  from the gauge set. The changes in the generator representation can be considered the reverse process of the S2G transformation. In practice, we only measure  $\hat{g}$  and apply the  $s_k$  operation if the result is 1. This does not affect the logical state, as  $s_k|P_{0/1}\rangle = |N_{0/1}\rangle$ .